A Stochastic Theory of the Hierarchical Clustering. III. The Nonuniversality and Nonstationarity of the Halo Mass Function

Andrea Lapi[1,2,3,4] , Tommaso Ronconi[1,2] , and Luigi Danese[1,2]
[1] SISSA, Via Bonomea 265, I-34136 Trieste, Italy; lapi@sissa.it
[2] IFPU—Institute for fundamental physics of the Universe, Via Beirut 2, I-34014 Trieste, Italy
[3] INFN-Sezione di Trieste, via Valerio 2, I-34127 Trieste, Italy
[4] INAF/IRA, Istituto di Radioastronomia, Via Piero Gobetti 101, I-40129 Bologna, Italy

Abstract

In the framework of the stochastic theory for hierarchical clustering, we investigate the time-dependent solutions of the Fokker–Planck equation describing the statistics of dark matter halos, and discuss the typical timescales needed for these to converge toward stationary states, far away enough from initial conditions. Although we show that the stationary solutions can reproduce the outcomes of state-of-the-art N-body simulations at $z \approx 0$ to great accuracy, one needs to go beyond to fully account for the cosmic evolution of the simulated halo mass function toward high redshift. Specifically, we demonstrate that the time-dependent solutions of the Fokker–Planck equation can describe, for reasonable initial conditions, the nonuniversal evolution of the simulated halo mass functions. Compared to standard theoretical estimates, our stochastic theory predicts a halo number density higher by a factor of several toward $z \gtrsim 10$, an outcome that can be helpful in elucidating early and upcoming data from JWST. Finally, we point out the relevance of our approach in designing, interpreting, and emulating present and future N-body experiments.

Unified Astronomy Thesaurus concepts: Cosmology (343); Dark matter (353)

1. Introduction

According to the standard cosmological framework, dark matter (DM) halos are thought to originate from the collapse of patches from an initial, close Gaussian perturbation field. However, as demonstrated by many extensive N-body simulations (e.g., see textbooks by Mo et al. 2010 and Cimatti et al. 2020 also comprehensive reviews by Vogelsberger et al. 2020; Angulo & Hahn 2022, and references therein), the detailed evolution of perturbations and (proto)halos ultimately depends on a variety of effects. First, the role of initial conditions is crucial, in that a perturbation is more prone to collapse if it resides within a sufficiently overdense region of the initial density field. This was actually the foundational idea of pioneering estimates for the halo abundance (see Press & Schechter 1974), subsequently refined in terms of the excursion set approach (see Bond et al. 1991; Lacey & Cole 1993; Mo & White 1996) to avoid the double counting of overdense regions overlapped with, or embedded within, larger collapsing ones (the so-called cloud-in-cloud issue).

In addition, the shape of (proto)halos may be also relevant, in that they tend to be ellipsoidal in shape (and especially so for smaller halos collapsing at late times), and this may influence the collapse efficiency and timescales (see Sheth & Tormen 1999, 2002). Moreover, collapse locations may be special points in the initial perturbation field, such as peaks in density or in energy (e.g., Bardeen et al. 1986; Paranjape & Sheth 2012; Lapi & Danese 2014; Musso & Sheth 2021). Finally, other nonlinear effects may influence the collapse of perturbations, such as mergers, tidal forces, dynamical friction, relaxation, local environment, angular momentum acquisition and dissipation, velocity fields, clumpiness, etc.; these involve different spatial/temporal scales, and enforce a considerable variance in the collapse of different (proto)halo patches in the universe.

Thus it should appear evident that the collapse and evolution of DM halos constitute an inherently stochastic process, originating not only from a degree of randomness in the initial conditions, but also from the complexity of deterministic processes affecting the ensuing collapse. As a consequence, the fine details of the evolution of individual halos at different spatial locations and cosmic times are, for all practical purposes, difficult to follow and/or model ab initio in (semi-)analytic terms. In this vein, Lapi & Danese (2020, 2021; hereafter LD20) have submitted that, if one is mainly interested in the statistical properties of the halo population as a whole, an effective description of (proto)halo collapse can be conveniently provided via a mean-field stochastic theory. Specifically, the average macroscopic dynamics of a (proto)halo mass $M(t)$ can be effectively described in terms of fluctuations driven by an appropriate noise term; the latter yields an average drift of the masses toward larger values, which renders the expected hierarchical clustering behavior of the halo population.

The situation is somewhat analogous to the classic description of Brownian motion: a microscopic particle immersed in a fluid continuously undergoes collisions with the fluid molecules; the resulting motion, despite being deterministic, appears to be random at the macroscopic level, especially to an external observer who has no access to the exact positions and velocities of the innumerable fluid molecules and to the initial conditions of the particle. In the way of a statistical description, the problem is effectively treated via a stochastic differential equation driven by a fluctuating white noise, which allows us to implicitly account for the complex microscopic dynamics of the system. Note that often the systems state influences the intensity of the driving noise, like when the Brownian

fluctuations of a microscopic particle near a wall are reduced by hydrodynamic interactions, so that the noise becomes multiplicative in terms of a nonuniform diffusion coefficient. Similar stochastic models with multiplicative noise have been employed to describe a wide range of physical phenomena, from Brownian motion in inhomogeneous media or in close approach to physical barriers, to thermal fluctuations in electronic circuits, to the evolution of stock prices, to computer science, to the heterogeneous response of biological systems and randomness in gene expression (e.g., Risken 1996; Mitzenmacher 2004; Reed & Jorgensen 2004; Paul & Baschnagel 2013). Note that in many contexts the validity of the stochastic equations designed on purpose to describe the macroscopic dynamics is checked by comparison with observations and/or numerical simulations. In the cosmological evolution of halos, N-body simulations provide the most relevant testbeds, although any comparison must be performed with care since their outcomes are dependent on many subtle details such as the limited number of simulated particles (i.e., mass resolution), the treatment of gravity on small scales (i.e., softening length), the sample statistics (i.e., simulated volumes), the background cosmology, etc.

In LD20 we have shown a preliminary comparison of the halo mass functions predicted by our stochastic theory with the results of a few classic N-body simulations, including Sheth & Tormen (1999); Bhattacharya et al. (2011), and Watson et al. (2013). The net outcome is that by appropriately gauging the parameters that regulate the mass and redshift dependence of the multiplicative noise term, our approach is capable of reproducing the simulation results, at least at $z \approx 0$. So far our analysis has been performed by only exploiting the stationary, steady-state solutions of the Fokker–Planck equation describing the stochastic dynamics; however, a detailed comparison with the most recent N-body simulations (e.g., Ishiyama et al. 2021; Shirasaki et al. 2021), which probe extended redshift and mass ranges, shows that one needs to go beyond. In particular, recent simulations have rekindled the interest and deepened the focus on the nonuniversality of the halo mass function; this means that the latter cannot be described in terms of a universal function $f(\nu)$ of a variable ν incorporating all its redshift and mass dependencies. Interpreting nonuniversality has proven a difficult task for standard approaches to the halo statistics, like the excursion set approach.

The main aim of the present work is to show that the nonuniversal behavior measured in simulations is naturally expected and quantitatively reproduced by our stochastic framework; specifically, it emerges whenever the solutions of the Fokker–Planck equation describing the stochastic dynamics have not yet converged to a stationary state, as it occurs for reasonable initial conditions in the standard cold DM cosmological framework. The plan of the paper is straightforward: in Section 2 we recall the basic formalism of our stochastic theory, focusing on nonstationary solutions of the Fokker–Planck equation and on the associated halo mass functions; in Section 3 we quantitatively compare stationary and nonstationary mass functions, and highlight that the latter can reproduce, for reasonable initial conditions, the nonuniversal behavior as measured in N-body simulations; in Section 4 we discuss and summarize our main findings. In the Appendix we present an approximate expression for the nonstationary solutions of the Fokker–Planck equation with space-dependent drift, which is exploited in the main text.

Throughout this work, we adopt the standard flat ΛCDM cosmology (Planck Collaboration et al. 2020) with rounded parameter values: matter density $\Omega_M = 0.3$, dark energy density $\Omega_\Lambda = 0.7$, baryon density $\Omega_b = 0.05$, Hubble constant $H_0 = 100\,h$ km s^{-1} Mpc^{-1} with $h = 0.7$, and mass variance $\sigma_8 = 0.8$ on a scale of $8\,h^{-1}$ Mpc.

2. Stochastic Theory of Hierarchical Clustering

In this section we recall the basics of the stochastic theory for hierarchical clustering developed in LD20; specifically, here we aim to highlight the intrinsic nonstationary behavior in the solutions of the Fokker–Planck equations, which regulate the halo mass function and its mass and redshift dependencies.

2.1. Basic Formalism

The proposal put forward by LD20 consists in describing the evolution of the halo population in terms of a stochastic formalism. In particular, the mass $M(t)$ of a (proto)halo patch is promoted to a variable fluctuating along the cosmic time t, as ruled by the stochastic differential equation (in the Stratonovich convention)

$$\frac{\mathrm{d}}{\mathrm{d}t}\,M = \frac{\sigma^2}{|\mathrm{d}\sigma/\mathrm{d}M|}\,\frac{1}{\delta_c(t)}\,\left|\frac{\dot{\delta}_c(t)}{\delta_c(t)}\right|^{1/2}\,\eta(t), \qquad (1)$$

where $\eta(t)$ is a Gaussian white noise with ensemble-average properties $\langle \eta(t) \rangle = 0$ and $\langle \eta(t)\eta(t') \rangle = 2\,\delta_D(t - t')$.

In the above equation, the quantity $\delta_c(t)$ is the critical threshold for collapse, which takes on present values around $\delta_c(t_0) \approx 1.68$ and scales with cosmic time t as $\delta_c(t) \propto D^{-1}(t)$ in terms of the growth factor $D(t)$ for linear perturbations. In addition, $\sigma(M)$ is the mass variance filtered on the scale M, defined as

$$\sigma^2(M) = \frac{1}{(2\pi)^3}\,\int \mathrm{d}^3k\,P(k)\,\tilde{W}_M^2(k), \qquad (2)$$

where $P(k)$ is the power spectrum of density fluctuation smoothed via a Fourier-transformed window function $\tilde{W}_M^2(k)$ whose volume in real space encloses the mass M; we note that any power spectrum or filter shapes can in principle be adopted in our framework. For definiteness, and in order to comply with choices largely implemented in N-body simulations, we employ hereafter the classic cold DM power spectrum by Bardeen et al. (1986). We also use the filter function proposed by Leo et al. (2018) with a smooth shape $\tilde{W}_M^2(k) \propto [1 + (k\,R_M)^{\omega_1}]^{-1}$, where the radius R_M is simply related to the mass M as $R_M \equiv (3\,M/4\,\pi\,\bar\rho)^{1/3}/\omega_2$ in terms of the average comoving matter density $\bar\rho$. For different parameters (ω_1, ω_2) such a general shape can mimic the behavior of the filters usually adopted in the literature: top-hat in real space, k − sharp (i.e., top-hat in Fourier space), Gaussian; we adopt the fiducial parameters $(\omega_1, \omega_2) = (4.8, 3.3)$ that are suggested by Leo et al. (2018) as the best choice for comparing with N-body mass functions. For the adopted power spectrum and filter shape, the relation $\sigma(M)$ from Equation (2) is purely deterministic, featuring an inverse, convex, slowly varying behavior.

Following LD20, the probability density $\mathcal{P}(M, t)$ for a region to enclose a mass between M and $M + dM$ at time t is

derived by solving the Fokker–Planck equation associated with Equation (1), which reads (see Appendix A of LD20 for a primer on Fokker–Planck equations)

$$\partial_t \mathcal{P}(M, t) = -\mathcal{T}^2(t) \partial_M [\mathcal{D}(M) \mathcal{D}'(M) \mathcal{P}(M, t)] + \mathcal{T}^2(t) \partial_M^2 [\mathcal{D}^2(M) \mathcal{P}(M, t)]], \quad (3)$$

where $\mathcal{D}(M) \equiv \sigma^2/|\mathrm{d}\sigma/\mathrm{d}M|$ and $\mathcal{T}(t) \equiv |\dot{\delta}_c|^{1/2}/\delta_c^{3/2}$. This must be supplemented by the natural boundary conditions $\mathcal{P}(\infty, t) = 0$ and $P(M, t) = 0$ for $M < 0$, and by an initial condition $\mathcal{P}(M, t_{in}) = \delta_D(M - M_{in})$ at a starting time $t_{in} < t$; the value M_{in} will be gauged against N-body simulations, as discussed in Section 3. Then the halo mass function is by definition related to the solution $\mathcal{P}(M, t)$ of the Fokker–Planck equation via

$$N(M, t) = \frac{\bar{\rho}}{M} \mathcal{P}(M, t). \quad (4)$$

The solution of Equation (3) can be obtained via a change of variables $X \equiv \int \mathrm{d}M / \mathcal{D}(M) = 1/\sigma$, $Y \equiv \int \mathrm{d}t \, \mathcal{T}^2(t) = 1/2 \, \delta_c^2$ and $\mathcal{W}(X, Y) \equiv \mathcal{D}(M) \mathcal{P}(M, t)$, in such a way that it reduces to a standard diffusion equation $\partial_Y \mathcal{W} = \partial_X^2 \mathcal{W}$. Taking into account the aforementioned boundary conditions and coming back to the original variables (see LD20 for details) one easily finds the solution via a Fourier transform:

$$\mathcal{P}(M, t) = \frac{\delta_c}{\sigma^2} \left| \frac{\mathrm{d}\sigma}{\mathrm{d}M} \right| \frac{1}{\sqrt{2\pi (1 - \delta_c^2 / \delta_{c,in}^2)}}$$
$$\times \left\{ \exp, \left[-\frac{\delta_c^2}{2\sigma^2} \frac{(1 - \sigma/\sigma_{in})^2}{1 - \delta_c^2/\delta_{c,in}^2} \right] \right.$$
$$\left. + \exp \left[-\frac{\delta_c^2}{2\sigma^2} \frac{(1 + \sigma/\sigma_{in})^2}{1 - \delta_c^2/\delta_{c,in}^2} \right] \right\} \quad (5)$$

where $\delta_{in} \equiv \delta_c(t_{in})$ and $\sigma_{in} = \sigma(M_{in})$. Far away from the initial conditions $t \gg t_{in}$ and $M \gg M_{in}$ one has that $\sigma \ll \sigma_{in}$ and $\delta_c \ll \delta_{c,in}$, to yield the stationary solution[5]

$$\mathcal{P}(M, t) = \sqrt{\frac{2}{\pi}} \frac{\delta_c}{\sigma^2} \left| \frac{\mathrm{d}\sigma}{\mathrm{d}M} \right| e^{-\delta_c^2/2\sigma^2}; \quad (6)$$

the related mass function after Equation (4) is found to be the formula originally suggested by Press & Schechter (1974), including the fudge factor of 2 in the normalization that in the literature is often justified via the excursion set approach (see Bond et al. 1991).

2.2. Multiplicative Noise

To add more complex stochastic dynamics that will be needed to fit the N-body mass functions and investigate universality, it is convenient to reformulate our theory in terms of the scaled variable $\nu \equiv \delta_c(t)/\sigma(M)$ and introduce a modulation of the noise term. The basic evolution equation becomes

---

[5] We stress that to attain stationarity the time derivative $\partial_t \mathcal{P}$ appearing on the left-hand side of Equation (3) must be negligible with respect to the terms on the right-hand side. To a crude approximation, such a condition is met when the timescale $t_{FP} \sim \mathcal{T}^{-2}(t) \propto \delta_c^3(t)/\dot{\delta}_c(t) \ll t$ gets substantially smaller than the cosmic time t. In the standard ΛCDM cosmology the scaling $\delta_c \propto t^{-\zeta}$ with $\zeta \sim 2/3 - 1/2$ holds in the matter or dark energy-dominated era, implying that stationarity may be attained only at sufficiently late times, typically far away from the initial t_{in}. In Section 3 we will estimate quantitatively the timescale for the solution to converge toward the stationary state by solving the time-dependent Fokker–Planck equation with multiplicative noise and appropriate initial conditions gauged on N-body simulations.

(see LD20 for details):

$$\frac{\mathrm{d}}{\mathrm{d}t} \nu = -\nu \left| \frac{\dot{\delta}_c}{\delta_c} \right| + \frac{\nu}{B(\nu)} \left| \frac{\dot{\delta}_c}{\delta_c} \right|^{1/2} \eta(t), \quad (7)$$

where $B(\nu)$ is a function that describes a mass/redshift dependence of the noise strength. In particular, changing the variable from ν to M, one easily recognizes that $B(\nu) = \nu$ exactly corresponds to Equation (1), and in such a case the stochastic quantity ν evolves following an Ornstein–Uhlenbeck process with additive noise. If $B(\nu) \neq \nu$ instead the noise becomes multiplicative, i.e., dependent on the system's state, adding more complex dynamics. A simple yet flexible choice for the function $B(\nu)$ is

$$B(\nu) = \sqrt{q} \, \nu \left[1 + \frac{\beta}{(\sqrt{q} \, \nu)^{2\gamma}} \right], \quad (8)$$

in terms of three parameters (q, β, γ) that will be set later on by comparison with the N-body mass functions. The above shape is also employed in the excursion set approach, where it renders a possible mass dependence in the critical threshold for collapse $\delta_c(M, t) \approx \delta_c(t) B(\nu)/\nu$. However, in our theory $B(\nu)$ is just a description for the mass/redshift dependence of the multiplicative noise, and other expressions may in principle be considered.

The mass function is plainly related to the distribution of ν values at any given cosmic time as

$$N(M, t) = \frac{\bar{\rho}}{M} \mathcal{P}(M, t) = \frac{\bar{\rho}}{M^2} \left| \frac{\mathrm{d}\ln\nu}{\mathrm{d}\ln M} \right| \nu \mathcal{P}(\nu, t); \quad (9)$$

the quantity $f(\nu, t) = \nu \mathcal{P}(\nu, t)$ is often referred to in the literature as the "multiplicity function." The mass function $N(M, t)$ is said to be "universal" if the multiplicity function is only a function of ν and has no explicit time dependence, meaning that the evolution in cosmic time is solely encapsulated into the scaled variable ν.

Analogously to Section 2.1, the probability distribution $P(\nu, t)$ can be derived from the Fokker–Planck equation associated with the stochastic Equation (7), which reads:

$$\partial_t \mathcal{P}(\nu, t) = \left| \frac{\dot{\delta}_c}{\delta_c} \right| \partial_\nu \left\{ \nu \mathcal{P}(\nu, t) + \frac{\nu}{B(\nu)} \partial_\nu \left[\frac{\nu}{B(\nu)} \mathcal{P}(\nu, t) \right] \right\}, \quad (10)$$

supplemented by boundary conditions $\mathcal{P}(\infty, t) = 0$ and $\mathcal{P}(\nu, t) = 0$ for $\nu < 0$, and by an initial condition $P(\nu, t_{in}) = \delta_D(\nu - \nu_{in})$ that will be gauged via N-body simulations (see Section 3). To solve Equation (10) it is useful to rescale the time in terms of a new variable $\tau \equiv -\ln(\delta_c/\delta_{c,in})$, introduce the stretched space variable $x \equiv \int \mathrm{d}\nu \, B(\nu)/\nu$, and define a new density $\mathcal{F} \equiv (\nu/B) \mathcal{P}$. In this way we turn the Fokker–Planck equation into the canonical form

$$\partial_\tau \mathcal{F}(x, \tau) = \partial_x [B(x) \mathcal{F}(x, \tau)] + \partial_x^2 \mathcal{F}(x, \tau). \quad (11)$$

For the simple case $B(\nu) = \nu$, for which actually the rescaling $x = \nu$ and $\mathcal{F} = \mathcal{P}$ have no effect, the time-dependent solution satisfying the aforementioned initial and boundary conditions can be found analytically via a simple Fourier transform; the

result reads

$$\mathcal{P}(\nu, t) = \frac{1}{\sqrt{2\pi(1-\xi)}}\left\{\exp\left[-\frac{(\nu - \nu_{\rm in}\sqrt{\xi})^2}{2(1-\xi)}\right]\right.$$
$$\left.+ \exp\left[-\frac{(\nu + \nu_{\rm in}\sqrt{\xi})^2}{2(1-\xi)}\right]\right\}, \qquad (12)$$

where $\xi \equiv e^{-2\tau} = \delta_c^2/\delta_{c,\rm in}^2$. Re-expressing $\nu = \delta_c/\sigma$ and $\nu_{\rm in} = \delta_{c,\rm in}/\sigma_{\rm in}$ and considering Equation (9) this is seen to be the very same expression in Equation (5). Far away from the initial conditions $\xi \ll 1$ applies, and the solution $\mathcal{P}(\nu, \infty) = \bar{\mathcal{P}}(\nu)$ converges to the stationary state $\bar{\mathcal{P}}(\nu) = \sqrt{2/\pi}\, e^{-\nu^2/2}$ yielding again the Press & Schechter (1974) mass function.

For nonlinear $B(\nu)$ the time-dependent Fokker–Planck equation does not admit analytic treatment, and one has to rely on numerical methods. Nevertheless, when the noise strength is just a perturbation over the linear case $B(\nu) \sim \nu$ as expected in the present context, it is possible to work out an expression that approximates the exact solution, along the lines developed in the Appendix. The result, taking into account the appropriate boundary conditions, reads

$$\mathcal{P}(\nu, t) = \frac{\mathcal{A}}{2\sqrt{1-\xi}}\frac{B(\nu)}{\nu}\left\{\exp\left[-\theta\frac{\sqrt{\xi}}{1-\xi}\frac{(x-x_{\rm in})^2}{2}\right]\right.$$
$$\left.+ \exp\left[-\theta\frac{\sqrt{\xi}}{1-\xi}\frac{(x+x_{\rm in})^2}{2}\right]\right\}$$
$$\times \exp\left\{-\frac{1}{1+\sqrt{\xi}}\int^\nu d\nu'\frac{B^2(\nu')}{\nu'} - \frac{\sqrt{\xi}}{1+\sqrt{\xi}}\int^{\nu_{\rm in}}d\nu'\frac{B^2(\nu')}{\nu'}+\right.$$
$$\left.+ \frac{\sqrt{\xi}}{1+\sqrt{\xi}}\frac{B^2(\nu_{\rm in})}{\theta} + \left[1 - \frac{1}{\theta}\frac{d\ln B(\nu)}{d\ln\nu}\right]\ln(1+\sqrt{\xi})\right\},$$
$$(13)$$

where $\xi \equiv e^{-2\theta\tau} = [\delta(t)/\delta(t_{\rm in})]^{2\theta}$, $x(\nu) \equiv \int^\nu d\nu' B(\nu')/\nu'$, $x_{\rm in} = x(\nu_{\rm in})$, the normalization constant $\mathcal{A}$ is determined by the condition $\int_0^\infty d\nu\,\mathcal{P} = 1$, and θ is a parameter controlling the intermediate time behavior of the solution (see Appendix for details). It is a matter of simple algebra to check that this solution reduces to Equation (12) in the case of $B(\nu) = \nu$. Note that hereafter we will always refer to and illustrate the results from numerically solving the time-dependent Fokker–Planck equation Equation (10), but we stress that the analytic formula Equation (13) is quite effective, approximating the exact solution within 15% in the relevant range of ν; therefore, after gauging the noise parameters (q, β, γ) and the initial condition $\nu_{\rm in}$ via N-body simulations (see Section 3), it can be used for quickly emulating their outputs, and for modeling/forecasting purposes in a galaxy formation context.

Far away from the initial conditions $\mathcal{P}(\nu, \infty) = \bar{\mathcal{P}}(\nu)$, the solution converges to the stationary state

$$\bar{\mathcal{P}}(\nu) = \mathcal{A}\frac{B(\nu)}{\nu}\exp\left[-\int^\nu d\nu'\frac{B^2(\nu')}{\nu'}\right], \qquad (14)$$

which has been originally derived in LD20 by a simple integration after setting $\partial_t\mathcal{P} = 0$ in Equation (10). We point out that in our stochastic framework the mass function will become universal only far away from initial conditions, when the stationary state $\bar{\mathcal{P}}(\nu)$ above is attained. However, at a generic cosmic time the solutions of the Fokker–Planck equation for reasonable initial conditions will feature an explicit time dependence in the multiplicity function $\nu\,\mathcal{P}(\nu, t)$, that will cause the mass function to break universality.

3. Comparison with *N*-body Mass Function: Nonuniversality as Nonstationarity?

We now aim to quantitatively show the difference between stationary and nonstationary solutions, and to check whether the latter can quantitatively render the nonuniversality measured in the N-body simulations.

As a preliminary step, we start by fitting[6] the multiplicity function at $z \approx 0$ extracted from the state-of-the-art N-body simulations by Shirasaki et al. (2021) with the stationary solution Equation (14), and perform maximum likelihood estimation on the parameters (q, β, γ) describing the noise strength in Equation (8). In Figures 1 and 2 (blue regions and lines) we illustrate the marginalized posterior distributions of the parameters (see also Table 1) and the resulting fit to the N-body multiplicity function at $z \approx 0$. The overall rendition of the simulated data (circles) is extremely good. In addition, the inset of Figure 2 shows that the fit is achieved with a minimal deviation from the simple case $B(\nu) = \nu$ (i.e., the mass and redshift dependence of the noise strength are minor) in the range of ν-values probed by simulations, though the difference in the multiplicity function from the corresponding Press & Schechter (1974) shape is appreciable.

Despite such an excellent performance, it is found that the halo mass function based on the stationary solution of the Fokker–Planck equation deviates appreciably from the N-body outcomes toward progressively higher redshifts; this is because, as highlighted in Figure 2, the simulated multiplicity function has a slight explicit dependence on cosmic time, making its shape at $z \gtrsim 1$ considerably different from that at $z \approx 0$ (e.g., see squares in Figure 2 referring to $z \approx 3$). As mentioned in Section 2, in our stochastic framework a natural explanation for this additional dependence could be that the solution $\mathcal{P}(\nu, t)$ of the time-dependent Fokker–Planck Equation (10) has not yet converged to the stationary state.

To test this hypothesis, we relax the assumption of stationarity and fit the Shirasaki et al. (2021) halo multiplicity function in the redshift range $z \approx 0 - 3$ with the time-dependent solution of the Fokker–Planck equation. To this purpose, besides the three parameters (q, β, γ) regulating the noise strength, we consider as an additional one the initial condition $\nu_{\rm in}$ needed to integrate Equation (10); the initial redshift is set at $z_{\rm in} \approx 100$ as in the simulations (anyway, we checked that the outcomes are marginally affected by the choice of $z_{\rm in}$ in the range 30–300).

In Figure 3 we show the MCMC marginalized distributions for the fitting parameters (see also Table 1). It is seen that the

---

6 For all the fits in the paper, we adopt flat priors on the parameters within the ranges $(q, \beta, \gamma) \in [0, 2]$ and $\log \nu_{\rm in} \in [-2, 2]$. Then we sample the posterior distributions via an MCMC technique, by running the Python package emcee with 10^4 steps and $N \times 100$ walkers where N is the number of fitting parameters. Each walker is initialized with a random position uniformly sampled from the (flat) priors. After checking the autocorrelation time, we remove the first 20% of the flattened chain to ensure burn-in; the typical acceptance fractions are of order 40%.
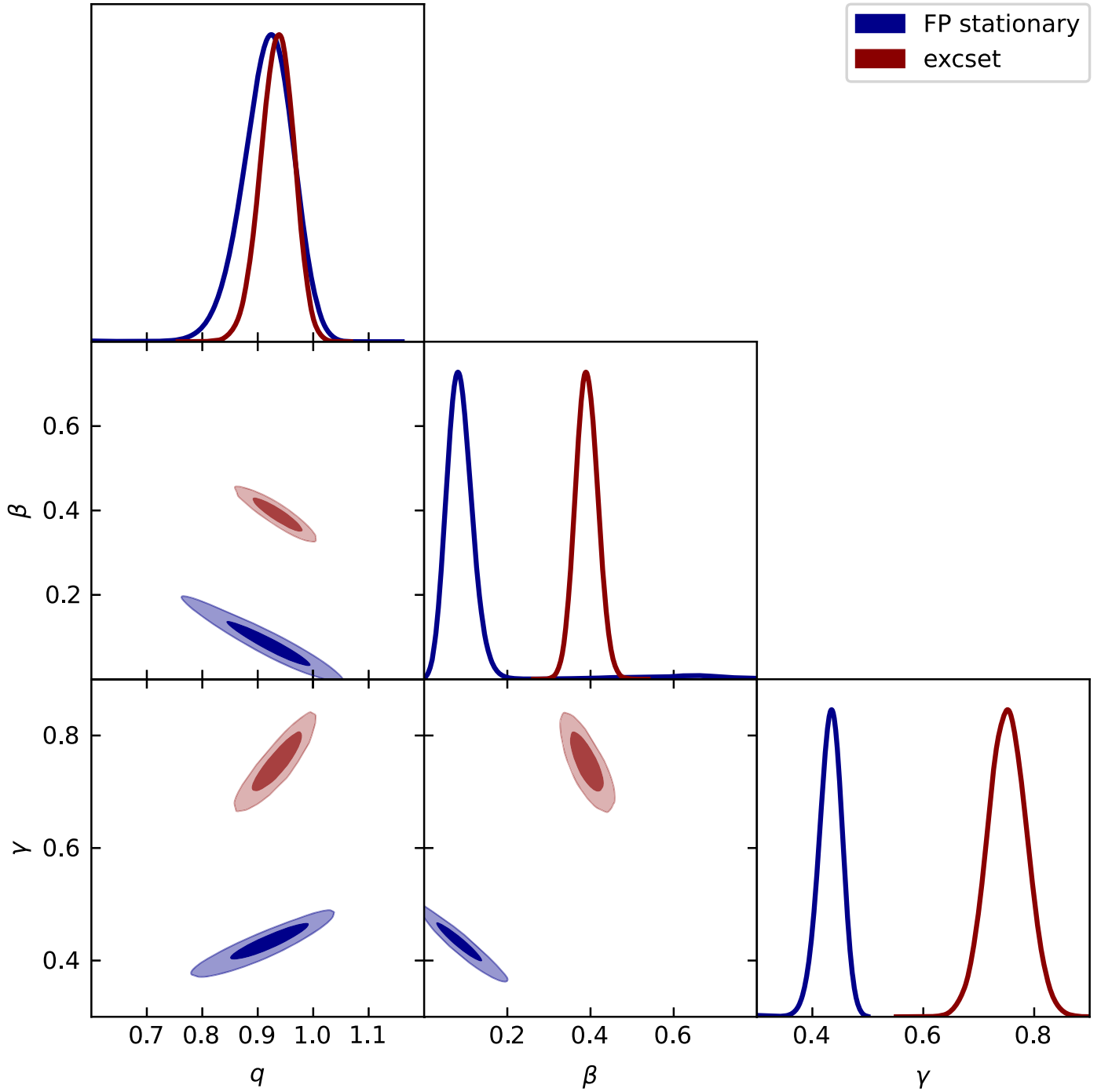
Figure 1. MCMC posterior distributions for the parameters triple (q, β, γ) ruling the mass/redshift dependence in Equation (8), obtained by fitting the halo multiplicity function at $z \approx 0$ by Shirasaki et al. (2021) via the stationary solutions of the Fokker–Planck equation (blue contours/lines; see Equation (14)), and via the excursion set approach (red contours/lines; see Equation (16)). Contours show 68% and 95% confidence intervals, and the marginalized distributions are in arbitrary units (normalized to 1 at their maximum value).

values (q, β, γ) are consistent within $\approx 2\sigma$ with those obtained fitting only the $z \approx 0$ multiplicity function with the stationary solution. As to the additional parameter ruling the initial condition, we find a value $\nu_{\rm in} = \delta_c(z_{\rm in})/\sigma(M_{\rm in}) \approx 3$; given the adopted initial redshift $z_{\rm in} \approx 100$ this corresponds to a very small (Earth-like) mass $M_{\rm in} \approx M_\oplus \approx 10^{-6} M_\odot$, which is pleasingly close to the free-streaming length of cold DM particles. On the one hand, this is an intriguing consistency check, since the cold nature of DM is a basic assumption of the simulations by Shirasaki et al. (2021), though the related mass resolution does not allow them to sample halos with mass below $10^5 M_\odot$. On the other hand, specific cold DM simulations focused on the very high-redshift universe have shown that the first structures to form in the standard cosmological framework are precisely Earth-like mass halos at $z_{\rm in} \approx 50$–150 (e.g., Hofmann et al. 2001; Green et al. 2004; Diemand et al. 2005; see also review by Angulo et al. 2022), in agreement with our findings.

In Figure 4 we illustrate the evolution with redshift of the multiplicity function associated with the numerical solution of the time-dependent Fokker–Planck equation, by assuming the
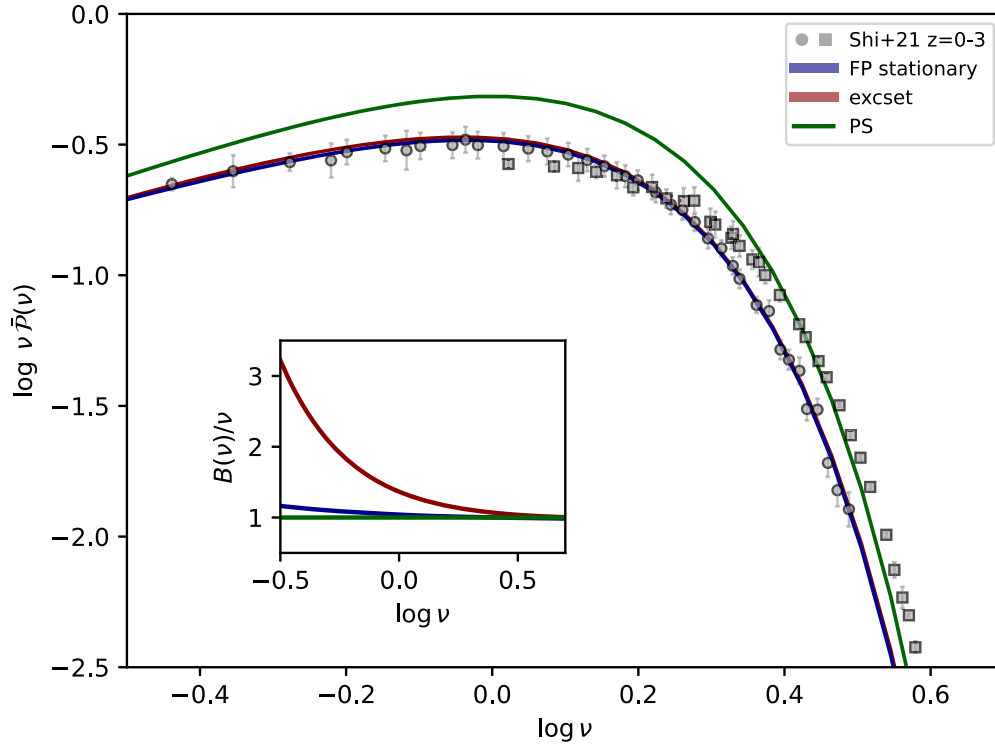
Figure 2. Fits to the halo multiplicity function by Shirasaki et al. (2021) at $z \approx 0$ (circles) with the stationary solution of the Fokker–Planck equation (see Equation (14); blue solid line), and with the excursion set approach (see Equation (16); red line). The Press & Schechter (1974) multiplicity function is also reported for reference (green lines). The nonuniversal behavior in the simulations is highlighted by the different shapes of the multiplicity function by Shirasaki et al. (2021) at $z \approx 3$ (squares). The inset shows the deviation of the noise strength (for the stochastic theory) or of the collapse threshold (excursion set) from the constant case yielding the Press & Schechter (1974) shape.

Table 1
Marginalized Posterior Estimates of the Parameters from the MCMC Analysis

Framework	q	β	γ	$\log \nu_{\rm in}$
FP—stationary	$0.89^{+0.07}_{-0.02}$	$0.11^{+0.01}_{-0.06}$	$0.42^{+0.03}_{-0.01}$	⋯
Excursion set	$0.94^{+0.03}_{-0.03}$	$0.39^{+0.03}_{-0.03}$	$0.75^{+0.04}_{-0.04}$	⋯
FP—time dependent	$0.89^{+0.01}_{-0.02}$	$0.05^{+0.01}_{-0.01}$	$0.47^{+0.01}_{-0.01}$	$0.48^{+0.03}_{-0.01}$

aforementioned best-fit parameters and initial condition. As time passes, the low-mass end (low ν values) of the multiplicity function monotonically flattens and extends toward smaller and smaller masses. Contrariwise, the behavior of the high-mass end (high ν values) first flattens and then steepens again, to produce the observed exponential suppression at low z. We highlight that stationarity is marginally attained by the full time-dependent solution only toward $z \approx 0$ (see magenta line); we stress that such an evolution is an outcome of the fitting procedure and not an a priori assumption. The implied timescale for the time-dependent solution to converge toward the stationary state amounts to many Gyr.

Finally, in Figure 5 (see green lines) we show that the overall evolution of the N-body halo mass function is well captured by our time-dependent solution, much better than by the stationary state, out to high redshift. Specifically, we report the N-body data by Shirasaki et al. (2021) out to $z \sim 6$, which is the maximal redshift where their results can be considered robust and do not suffer from volume sampling issues. Our nonstationary solution reproduces very well the evolution of the $N-$body mass function. This is even more remarkable

considering that the evolution of the nonstationary solutions depends mainly on one parameter, namely the initial condition $\nu_{\rm in}$, that has been calibrated by fitting the evolution of the N-body multiplicity function over the redshift range $z \lesssim 3$. As for higher redshifts $z \gtrsim 10$, Behroozi et al. (2013, 2020) worked out an educated recalibration and extrapolation of the N-body mass function from the Tinker et al. (2008) simulations; interestingly, their inference falls very close to the nonstationary solution provided by our theory.

We stress that at $z \sim 6$ the discrepancy between the stationary and nonstationary solutions amounts to a factor of a few over the whole range of relevant masses, and this increases to a factor of several or more toward higher $z \gtrsim 10$. Such a difference may have profound implications in the astrophysical and cosmological interpretation of high-redshift data from galaxy surveys, like those that will be conducted via the JWST.

3.1. Stochastic Theory versus Excursion Set Approach

The excursion set approach has been and is still widely exploited in order to investigate the evolution of the halo mass function; thus it is natural to compare its foundations and outcomes to those of our stochastic theory. The excursion set framework is based on the ansatz that the mass function is given by

$$N(M, t) = \frac{\bar{\rho}}{M^2} \left| \frac{{\rm d}\ln S}{{\rm d}\ln M} \right| S f_{\rm FC}(S), \qquad (15)$$
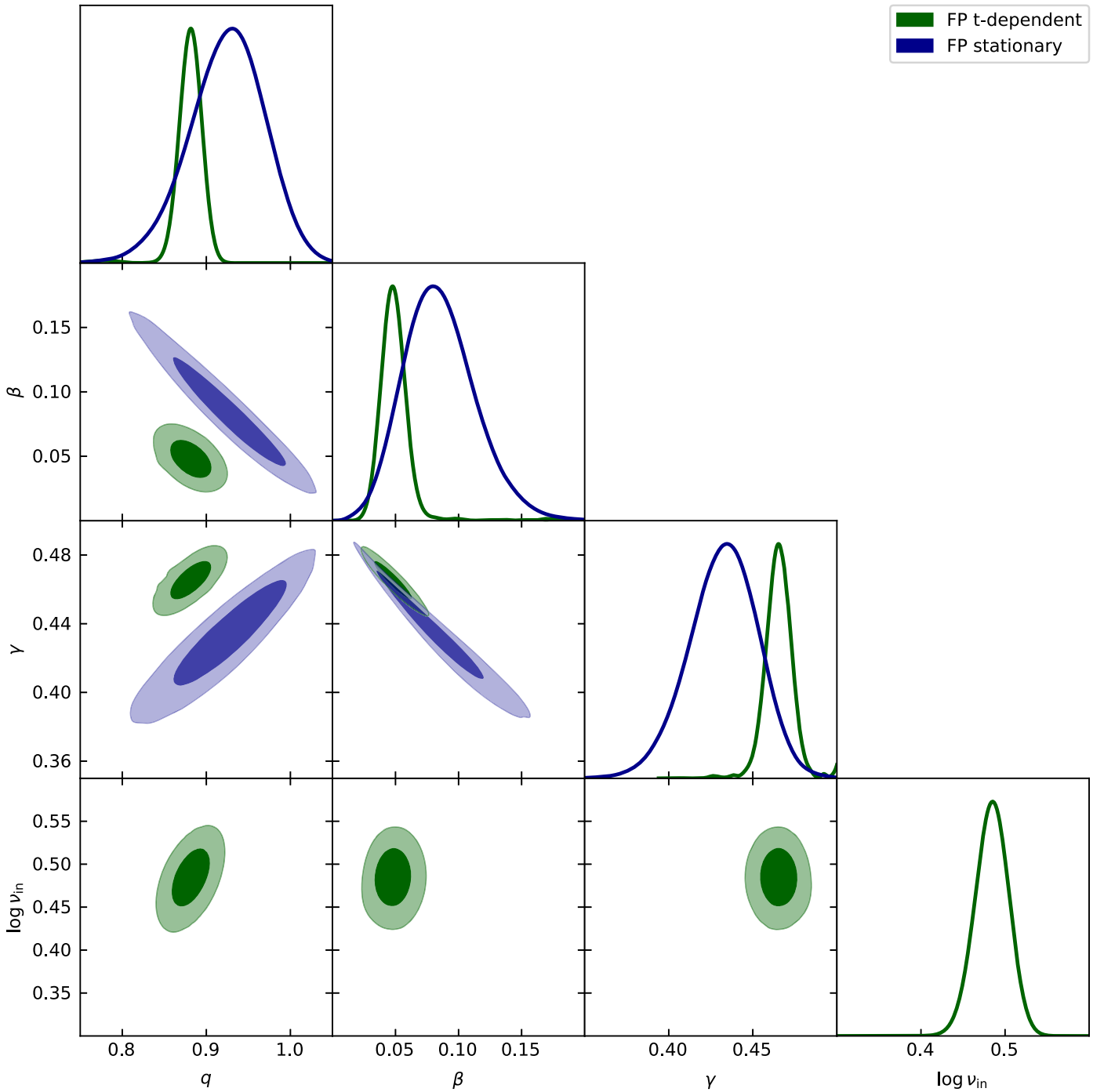
Figure 3. MCMC posterior distributions for the parameters triple (q, β, γ) ruling the mass/redshift dependence in Equation (8) and the initial condition ν_{in} set at $z_{in} \approx 100$, obtained by fitting the halo multiplicity function by Shirasaki et al. (2021) in the redshift range $z \approx 0$–3 via the time-dependent solutions of the Fokker–Planck equation (green contours/lines; see Equation (13)). For comparison, the posterior distributions on (q, β, γ) for the fit via the stationary solution of the Fokker–Planck equation are reported in Figure 1 (blue contours/lines). Contours show 68% and 95% confidence intervals, and the marginalized distributions are in arbitrary units (normalized to 1 at their maximum value).

where $S \equiv \sigma^2$, and $f_{FC}(S)$ represents the first crossing distribution of the random trajectories $\delta(S)$ across the moving barrier $\delta_c(t)B(\nu)/\nu = \sqrt{S}\,B(\nu)$. Note that such random walks are Markovian paths driven by white noise only when a sharp filter in Fourier space is adopted in the definition of $\sigma(M)$ via Equation (2); this is the common choice in the excursion set approach, despite the technical difficulties in normalizing the filter and localizing it in real space (see Mo et al. 2010 for an educated discussion). Often in the literature the same shape in Equation (8) is adopted, and in this context it is interpreted as a mass-dependent threshold due to the ellipsoidal collapse of perturbations. However, a relevant remark is that working in the abstract $\delta - S$ space (i.e., looking for the first crossing of a time-dependent barrier by a random walk) forces us to consider the multiplicity and mass functions as a sequence of stationary states, the evolution in time being solely dictated by the

Time Evolution of the Multiplicity function
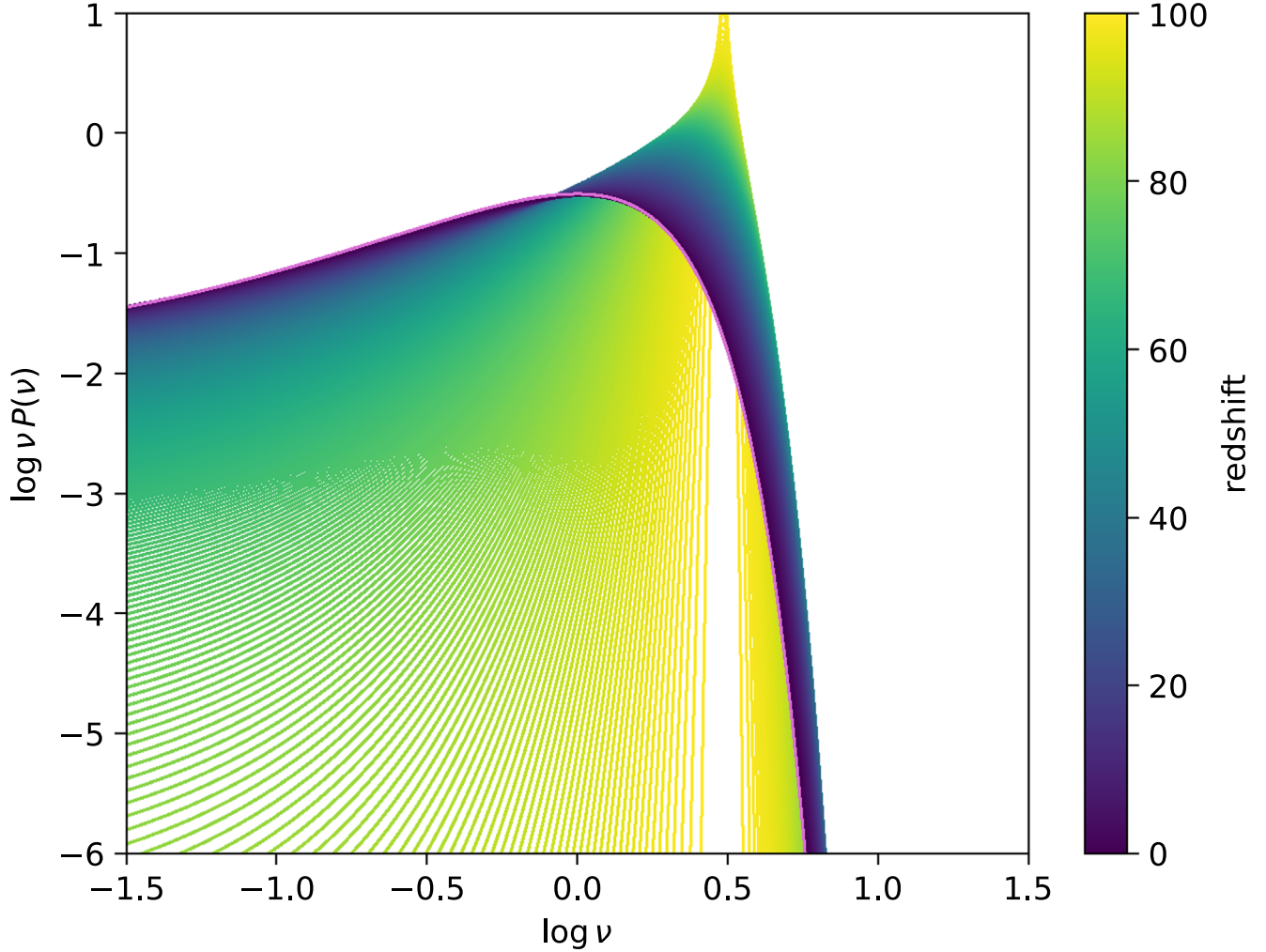
Figure 4. The overall evolution of the time-dependent solutions of the Fokker–Planck equation; fitting parameters (q, β, γ, ν_{in}) have been set at the mean posterior values from the previous Figure (see also Table 1). Colored lines are for different redshifts from $z_{in} \approx 100$ down to $z \approx 0$ as illustrated by the color bar. The magenta line shows the corresponding stationary state.

progressive decrease of the barrier following the growth factor $\delta_c(t) \propto D^{-1}(t)$. As a consequence, the outcomes of the excursion set approach can be compared only to the stationary solutions obtained via our stochastic theory; moreover, plainly in the excursion set framework the nonuniversality of the mass function cannot be interpreted as nonstationarity.

The solution to the first crossing problem[7] is implicitly given by the Volterra integral equation (see Lapi et al. 2013)

$$\mathrm{erfc}\left[\frac{B(S)}{\sqrt{2\,S}}\right] = \int_0^S \mathrm{d}\,S'\, f_{FC}(S')\,\mathrm{erfc}\left[\frac{B(S)-B(S')}{\sqrt{2(S-S')}}\right]. \quad (16)$$

One of the few cases solvable analytically is the linear barrier $B_{\gamma=1}(S) = \sqrt{q}\,\delta_c + \beta\,S/\sqrt{q}\,\delta_c$ that corresponds to $\gamma = 1$ in Equation (8); the solution obtained via Laplace transforms is

---

[7] Interestingly, from a historical perspective, the problem of finding the first crossing distribution to a constant barrier for a Brownian motion has been solved very early in the past century (since the first attempts by Bachelier 1900) and many studies have been subsequently dedicated to generalize the solution for more general "moving" boundaries (e.g., Tuckwell & Wan 1984; Durbin 1985 for a review see Grebenkov 2015).

the inverse Gaussian distribution $f_{FC}(S) = \sqrt{q}\,\delta_c/\sqrt{2\pi\,S^3} \times e^{-B_{\gamma=1}^2(S)/2\,S}$. For generic nonlinear barriers, one must rely on numerical techniques for solving Equation (16), like the recursive method by Zhang & Hui (2006). In the specific case of constant barrier ($q = 1$ and $\beta = 0$), the Press & Schechter (1974) mass function is recovered, which is the same outcome of the stochastic theory (in stationary conditions). This is due to a curious circumstance first pointed out by Bond et al. (1991) see their Equations (3).5 and 3.9: the first crossing distribution for a constant barrier can be derived from the solution of a diffusion equation, which is analogous to that of the stochastic theory (see Section 2.1).

One may ask whether the excursion set approach and our stochastic theory (for stationary solutions) produce the same results with a generic barrier like that in Equation (8). To this purpose we have exploited Equation (16) to fit the multiplicity function at $z \approx 0$ by Shirasaki et al. (2021) with the excursion set formalism, obtaining the results reported in Figure 1 and Figure 2 as red lines/contours (see also Table 1). Despite the fact that the multiplicity function is fitted comparably well with respect to our stochastic

Halo Mass Function
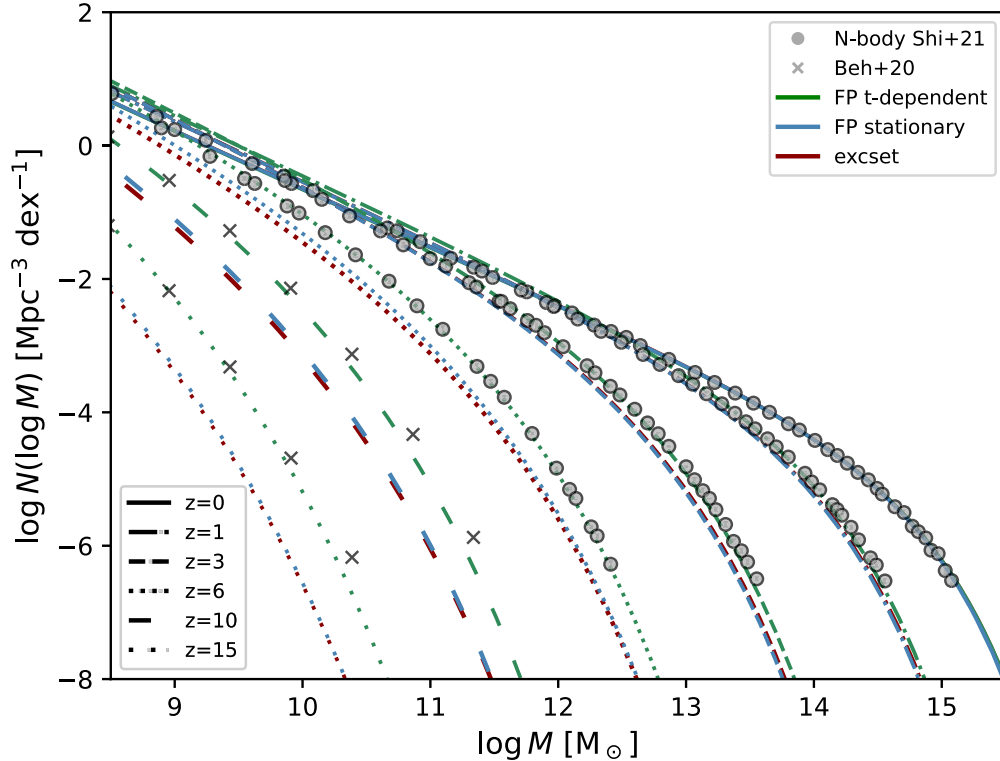
Figure 5. Halo mass function at redshifts $z = 0$ (solid), 1 (dotted–dashed), 3 (dashed), 6 (dotted), 10 (loosely dashed), and 15 (loosely dotted). The best-fit rendition from the time-dependent (green lines) and stationary (blue lines) solutions of the Fokker–Planck equation, and from the excursion set framework (red lines, very close to the blue ones), are compared with the outcomes from the N-body simulations by Shirasaki et al. (2021; gray circles) at $z \lesssim 6$. For higher redshift $z \gtrsim 10$ we also report (sampled in 0.5 dex mass logarithmic bins) the inference by Behroozi et al. (2013, 2020; gray crosses), which is an educated recalibration and extrapolation of the Tinker et al. (2008) simulations.

theory, the excursion set approach requires the threshold for collapse to deviate substantially from the constant one (see inset), especially toward low-mass halos and/or late times. On the one hand, the marginalized parameter values appreciably deviate from those (1, 0.47, 0.615) expected from the ellipsoidal collapse of perturbations, somewhat questioning such a classic view (see Sheth & Tormen 2002; Mo et al. 2010). On the other hand, interpreting Equation (8) as providing a mass and redshift-dependent collapse threshold can cause a theoretical pitfall: the barrier required to fit simulations (see inset of 2) would imply a significant evolution in time at fixed mass, putting additional concerns on the implicit assumption of stationarity. Finally, as shown in Figure 5 (red lines), the excursion set framework produces intrinsically stationary solutions, that cannot explain the nonuniversal evolution of the mass function toward high redshift.

4. Summary

In this paper we have investigated, in the framework of the stochastic theory for hierarchical clustering developed by LD20, the time-dependent solutions of the Fokker–Planck equation describing the statistics of dark matter halos. We have shown that, for reasonable initial conditions, quite long timescales of order many Gyr are needed for such solutions to converge toward stationary states.

Although the stationary solutions can reproduce the outcomes of state-of-the-art N-body simulations at $z \approx 0$ to great accuracy, requiring only a marginal dependence of the noise strength on halo mass and redshift, one needs to go beyond

them to fully account for the detailed dependence on cosmic time of the simulated halo mass function. This is because the latter is found to be not strictly universal; in a sense it cannot be completely characterized in terms of a function $f(\nu)$ of a scaled variable $\nu \equiv \delta_c(t)/\sigma(M)$ encapsulating all the mass and redshift dependence via the collapse threshold $\delta_c(t)$ and the mass variance $\sigma(M)$. We have demonstrated that the time-dependent, nonstationary solutions of our stochastic theory can quantitatively reproduce, for reasonable initial conditions in the standard cosmological framework, such as nonuniversality and the detailed redshift dependence of the halo mass functions as measured in state-of-the-art N-body simulations.

Note that the issue of nonuniversality has been proved extremely difficult to clear in different approaches, like the standard excursion set framework. In the latter, the basic connection between the halo mass function and the first crossing distribution of a random walk hitting a mass and time-dependent barrier requires the implicit assumption of stationarity; this inevitably leads to a universal behavior in the halo statistics. Contrariwise, our stochastic theory allows for a natural and physical interpretation of the nonuniversality, just overwhelming any assumption of stationarity, and elucidating that to reach stationary states requires many Gyr.

As a consequence, nonstationary and stationary solutions yield halo mass functions with appreciable differences at increasing redshift, amounting to a factor of a few at $z \sim 6$ and several or more at $z \gtrsim 10$. On the one hand, such a difference could be further tested with N-body simulations probing an

extended mass range at these substantial redshifts, which are currently challenging but will be within reach of upcoming exascale supercomputing facilities. On the other hand, the nonstationarity in the halo mass function at high $z \gtrsim 10$ could be tested, though indirectly (linking luminous to dark matter is a delicate and uncertain procedure), by estimating observationally the abundance and clustering of first stars and primeval galaxies, a task that will be achieved via the analysis of JWST data (e.g., Harikane et al. 2022).

In a future perspective, the nonstationary and nonuniversal halo mass function from our stochastic theory could be helpful in designing, interpreting, and emulating N-body experiments with specific characteristics in the initial conditions, space and time resolutions, power spectra (e.g., related to nonstandard DM scenarios) and cosmological background (e.g., modified gravity theories).

Appendix
Approximate Solution of the Time-dependent Fokker–Planck Equation

In this Appendix we aim to obtain analytic expressions that approximate, uniformly in space and time, the solutions of the time-dependent Fokker–Planck equation (see Martin et al. 2019). We focus on the case of a constant diffusion coefficient (one can take it equal to 1, without loss of generality) and space-dependent drift so the Fokker–Planck equation to solve is

$$\partial_\tau \mathcal{F}(x, \tau) = \partial_x [B(x)\mathcal{F}(x, \tau)] + \partial_x^2 \mathcal{F}(x, \tau) ; \qquad (A1)$$

with initial condition $\mathcal{F}(x, \tau_{in}) = \delta_D(x - x_{in})$. This is Equation (11) of the main text.

First, we consider the stationary solution of Equation (A1), which can be derived by setting $\partial_\tau \mathcal{F} = 0$; it reads

$$\bar{\mathcal{F}}(x) \propto \exp \left\{ -\int^x dx' \, B(x') \right\}. \qquad (A2)$$

Then we introduce the function

$$\mathcal{G}(x, \tau) \equiv \frac{\mathcal{F}(x, \tau)}{\bar{\mathcal{F}}(x)}, \qquad (A3)$$

that is easily seen to satisfy the backward Fokker–Planck equation

$$\partial_\tau \mathcal{G}(x, \tau) = -B(x)\partial_x \mathcal{G}(x, \tau) + \partial_x^2 \mathcal{G}(x, \tau). \qquad (A4)$$

We now define the function

$$\mathcal{H}(x, \tau) \equiv -\partial_x \ln \mathcal{G}(x, \tau), \qquad (A5)$$

which is found to satisfy a Burgers-like equation

$$\partial_\tau \mathcal{H}(x, \tau) = \partial_x [-B(x)\mathcal{H}(x, \tau) - \mathcal{H}^2(x, \tau) + \partial_x \mathcal{H}(x, \tau)]. \qquad (A6)$$

For the simple case $B(x) = \theta x$ it is easily verified by substitution in Equation (A6) that the solution is

$$\mathcal{H}(x, \tau) = \theta \frac{\xi x - \sqrt{\xi} x_{in}}{1 - \xi} = \theta \frac{\sqrt{\xi}}{1 - \xi}(x - x_{in}) - \frac{\sqrt{\xi}}{1 + \sqrt{\xi}} \tag{A7}$$

with $\xi \equiv e^{-2\theta\tau}$. The first term in the last expression is dominant for $\tau \to 0$ (or $\xi \to 1$), yielding $\mathcal{H}(x, \tau) \simeq (x - x_{in})/2\tau$ which for the original density $\mathcal{F}$ corresponds to the initial condition of a Dirac delta centered in x_{in}. This term must always be present also for general $B(x)$; hence we are led to make the ansatz

$$\mathcal{H}(x, \tau) \simeq \theta \frac{\sqrt{\xi}}{1 - \xi}(x - x_{in}) - \frac{\sqrt{\xi}}{1 + \sqrt{\xi}} B(x). \qquad (A8)$$

Remarkably, when inserting this expression into Equation (A6) and Laurent expanding around $\tau \to 0$, the l.h.s. and r.h.s. agree at orders τ^{-2} and τ^{-1}, so that the ansatz is correct at order τ^0 in the short-time limit (in principle one could improve the approximation by adding a Taylor series around $\tau = 0$ on the r.h.s. of Equation (A8), but we will not pursue this here). However, note that now the expansion of Equation (A8) reads $\mathcal{H}(x, \tau) \simeq (x - x_{in})/2\tau + B(x)/2$ so it is actually independent of θ; this means that θ is arbitrary in some sense and must be inferred by some other means. We will come back to this issue below.

We now determine $\mathcal{G}$, up to a time-dependent normalization constant, by integrating Equation (A5), to yield

$$\mathcal{G}(x, \tau) \simeq \mathcal{N}(\tau) \exp \left\{ -\int_{x_{in}}^x dx' \, \mathcal{H}(x', \tau) \right\}. \qquad (A9)$$

Using the expression for $\mathcal{H}(x, \tau)$ from Equation (A8) we get

$$\mathcal{G}(x, \tau) \simeq \mathcal{N}(\tau) \exp \left\{ -\theta \frac{\sqrt{\xi}}{1 - \xi} \frac{(x - x_{in})^2}{2} \right. $$
$$\left. + \frac{\sqrt{\xi}}{1 + \sqrt{\xi}} \int_{x_{in}}^x dx' \, B(x') \right\}. \qquad (A10)$$

The dependence on the starting point x_{in} in the normalization constant can be elicited by inserting Equation (A9) in Equation (A4) and obtaining the first-order differential equation

$$\frac{\dot{\mathcal{N}}}{\mathcal{N}} = \int_{x_{in}}^x dx' \, \partial_\tau \mathcal{H}(x', \tau) + B(x)\mathcal{H}(x, \tau)$$
$$- \partial_x \mathcal{H}(x, \tau) + \mathcal{H}^2(x, \tau). \qquad (A11)$$

The r.h.s. appears also to depend on x but actually do not; in fact, using Equation (A6) and considering that by definition

$\mathcal{N}(\tau) \to 1$ for $\tau \to \infty$ one finds

$$\mathcal{N}(\tau) = \exp\left\{\int_\tau^\infty d\tau'[-B(x)\mathcal{H}(x, \tau') \right.$$
$$\left. + \partial_x \mathcal{H}(x, \tau') - \mathcal{H}^2(x, \tau')]|_{x=x_{in}}\right\}. \quad (A12)$$

Exploiting now the explicit form of $\mathcal{H}(x, \tau)$ given by Equation (A8), after some algebra, one finds

$$\mathcal{N}(\tau) = \frac{1}{\sqrt{1-\xi}}\exp\left\{\frac{\sqrt{\xi}}{1+\sqrt{\xi}}\frac{B^2(x_{in})}{\theta} \right.$$
$$\left. + \left[1 - \frac{B'(x_{in})}{\theta}\right]\ln(1+\sqrt{\xi})\right\}. \quad (A13)$$

Using the above normalization in Equation (A10), and combining Equations (A2) and (A3) we obtain

$$\mathcal{F}(x, \tau) \propto \frac{1}{\sqrt{1-\xi}}\exp\left\{-\theta\frac{\sqrt{\xi}}{1-\xi}\frac{(x-x_{in})^2}{2} - \frac{1}{1+\sqrt{\xi}}\right.$$
$$\times \int^x dx' B(x') - \frac{\sqrt{\xi}}{1+\sqrt{\xi}}\int^{x_{in}} dx' B(x')$$
$$\left. + \frac{\sqrt{\xi}}{1+\sqrt{\xi}}\frac{B^2(x_{in})}{\theta} + \left[1 - \frac{B'(x_{in})}{\theta}\right]\ln(1+\sqrt{\xi})\right\}. \quad (A14)$$

We are now left with the problem of inferring the parameter θ, which controls the intermediate time behavior of the solution. One can argue to choose θ so as to minimize the error in the expansion underlying Equation (A8), that occurs for $B'(x) \simeq \theta$; this suggests taking

$$\theta \simeq \int dx\, \bar{\mathcal{F}}(x)B'(x), \quad (A15)$$

in terms of the steady-state solution $\bar{\mathcal{F}}(x)$. It is straightforward to verify that for $B(x) = x$ the above yields $\theta = 1$ and Equation (A14) collapses into the form

$$\mathcal{F}(x, \tau) \propto \frac{1}{\sqrt{1-\xi}}\exp\left\{-\frac{(x-\sqrt{\xi}\,x_{in})^2}{2(1-\xi)}\right\}; \quad (A16)$$

this is in fact the classic solution for the Fokker–Planck equation with constant diffusion coefficient and linear drift, which corresponds to an Ornstein–Uhlenbeck stochastic process with additive noise.

ORCID iDs

Andrea Lapi ⬤ https://orcid.org/0000-0002-4882-1735
Tommaso Ronconi ⬤ https://orcid.org/0000-0002-3515-6801
Luigi Danese ⬤ https://orcid.org/0000-0003-1186-8430

References

Angulo, R. E., & Hahn, O. 2022, LRCA, 8, 1
Planck Collaboration, Aghanim, N., Akrami, Y., et al. 2020, A&A, 641, A6
Bardeen, J. M., Bond, J. R., Kaiser, N., & Szalay, A. S. 1986, ApJ, 304, 15
Behroozi, P., Conroy, C., Wechsler, R. H., et al. 2020, MNRAS, 499, 5702
Behroozi, P. S., Wechsler, R. H., & Conroy, C. 2013, ApJ, 770, 57
Bhattacharya, S., Heitmann, K., White, M., et al. 2011, ApJ, 732, 122
Bond, J. R., Cole, S., Efstathiou, G., & Kaiser, N. 1991, ApJ, 379, 440
Cimatti, A., Fraternali, F., & Nipoti, C. 2020, Introduction to Galaxy Formation and Evolution (Cambridge: Cambridge Univ. Press)
Diemand, J., Moore, B., & Stadel, J. 2005, Natur, 433, 389
Durbin, J. 1985, J. Appl. Prob., 22, 99
Grebenkov, D. S. 2015, JPhA, 48, 013001
Green, A. M., Hofmann, S., & Schwarz, D. J. 2004, MNRAS, 353, L23
Harikane, Y., Ouchi, M., Oguri, M., et al. 2022, ApJS, submitted, arXiv:2208.01612
Hofmann, S., Schwarz, D. J., & Stocker, H. 2001, PRD, 64, 083507
Ishiyama, T., Prada, F., Klypin, A. A., et al. 2021, MNRAS, 506, 4210
Lacey, C., & Cole, S. 1993, MNRAS, 262, 627
Lapi, A., & Danese, L. 2014, JCAP, 07, 044
Lapi, A., & Danese, L. 2020, ApJ, 903, 117, [LD20]
Lapi, A., & Danese, L. 2021, ApJ, 911, 11
Lapi, A., Salucci, P., & Danese, L. 2013, ApJ, 772, 85
Leo, M., Baugh, C. M., Li, B., & Pascoli, S. 2018, JCAP, 04, 10
Martin, R. J., Craster, R. V., Pannier, A., & Kearney, M. J. 2019, J. Phys. A: Math. Theor., 52, 085002
Mitzenmacher, M. 2004, Internet Math., 1, 226
Mo, H., van den Bosch, F., & White, S. D. M. 2010, Galaxy Formation and Evolution (Cambridge: Cambridge Univ. Press)
Mo, H. J., & White, S. D. M. 1996, MNRAS, 282, 347
Musso, M., & Sheth, R. K. 2021, MNRAS, 508, 3634
Paranjape, A., & Sheth, R. K. 2012, MNRAS, 426, 2789
Paul, W., & Baschnagel, J. 2013, Stochastic Processes from Physics to Finance (Berlin: Springer)
Press, W. H., & Schechter, P. 1974, ApJ, 187, 425
Reed, W. J., & Jorgensen, M. 2004, Commun. Stat., 33, 1733
Risken, H. 1996, The Fokker–Planck Equation: Methods of Solution and Applications (Berlin: Springer)
Sheth, R. K., & Tormen, G. 1999, MNRAS, 308, 119
Sheth, R. K., & Tormen, G. 2002, MNRAS, 329, 61
Shirasaki, M., Ishiyama, T., & Ando, S. 2021, ApJ, 922, 89
Tinker, J., Kravtsov, A. V., Klypin, A., et al. 2008, ApJ, 688, 709
Tuckwell, H. C., & Wan, F. Y. M. 1984, J. Appl. Prob., 21, 695709
Vogelsberger, M., Marinacci, F., Torrey, P., & Puchwein, E. 2020, NatRP, 2, 42
Watson, W. A., Iliev, I. T., D?Aloisio, A., et al. 2013, MNRAS, 433, 1230
Zhang, J., & Hui, L. 2006, ApJ, 641, 641